Draft version March 10, 2018
Preprint typeset using LaTeX style AASTeX6 v. 1.0

NON-ZEEMAN CIRCULAR POLARIZATION OF MOLECULAR SPECTRAL LINES IN THE ISM

M. A. Chamma[1], M. Houde[1], J. M. Girart[2] and R. Rao[3]
[1]Department of Physics and Astronomy, The University of Western Ontario, London, ON, N6A 3K7, Canada
[2]Institut de Ciències de l'Espai (IEEC-CSIC), Can Magrans, S/N, E-08193 Cerdanyola del Vallès, Catalonia, Spain
and
[3]Submillimeter Array, Academia Sinica Institute of Astronomy and Astrophysics, 645 N. Aohoku Place, Hilo, HI 96720, USA

Abstract

We searched archival data of the Submillimeter Array (SMA) for evidence of circular polarization in common molecular tracers, most notably CO. This circular polarization possibly arises from anisotropic resonant scattering, which would imply that some background linearly polarized flux is being converted to circular polarization. We find circular polarization in NGC7538, IRC+10216 and Orion KL for transitions of CO, SiO, SiS, and $H^{13}CN$ at high enough levels to suggest that the presence of circular polarization in these spectral lines is common for such objects. This would imply that an important piece of information has been missed when studying magnetic fields through linear polarization from molecular spectral lines in the interstellar medium.

1. INTRODUCTION

Understanding the role of magnetic fields in star-forming regions allows us to test ideas about free-fall collapse and support mechanisms in molecular clouds, filling in details about the star formation process. Since we can only measure the radiation from star-forming regions astronomers use polarimetry to infer the magnitude and orientation of the magnetic field. The Davis-Chandrasekhar-Fermi (DCF) (Chandrasekhar & Fermi 1953) uses the dispersion of polarization angles (PA) of linear polarization (LP) for such studies[I don't understand Martin's note here] to obtain corresponding maps of the plane-of-the-sky component of the magnetic field. The presence of a magnetic field leads to linearly polarized radiation because dust and molecules will align themselves relative to the field. Aligned particles can emit radiation with a net level of linear polarization greater than zero. Aligned dust can also absorb radiation whose polarization is aligned with its long axis, acting as a sort of polarizing grid. Thus measuring the amount of dust linear polarization in the infrared continuum tells us about the degree to which the dust is aligned with the magnetic field, which in turn can tell us about the strength of the magnetic field (Chandrasekhar & Fermi 1953; Crutcher 2012).

The alignment of molecules and their interaction with the ambient magnetic field can cause that molecule's transitions to be linearly polarized by a few percent through the so-called Goldreich-Kylafis effect (Goldreich & Kylafis 1981). As with dust, the PA associated with the linear polarization in the spectral line can be measured and used to infer properties of the magnetic field through a dispersion analysis (Chandrasekhar & Fermi 1953; Crutcher 2012).

For molecular lines circular polarization is usually ignored, largely because of difficulty in its measurement and its assumed irrelevance. However, a significant amount of unexpected circular polarization was reported by Houde et al. (2013) in a rotational transition of CO using the Caltech Submillimeter Observatory (CSO), a common tracer through LP of magnetic fields (Crutcher 2012). The presence of circular polarization in a molecular transition can be explained with Zeeman splitting for some molecules/transitions possessing a significant magnetic moment (e.g., CN), but CO is highly insensitive to the Zeeman effect. In addition, the observed Stokes V profile in Orion KL was positive and symmetric, which is also unexpected since Zeeman splitting usually gives rise to an approximately antisymmetric Stokes V profile. To explain this detection a model was proposed whereby linearly polarized light is converted to circularly polarized light through anisotropic resonant scattering (ARS) (Houde et al. 2013; Houde 2014). This was further tested in the supernova remnant IC443 by Hezareh et al. (2013) where the measured CP flux of CO lines ($J = 2 \rightarrow 1$) and ($J = 1 \rightarrow 0$) were 're-inserted' into the measured LP flux to account for the LP-to-CP conversion and its effect on the PA. They found that the PAs obtained from

different CO transitions only agreed with each other and those obtained from dust polarimetry after the CP flux was accounted for. If ARS is common to other objects then using LP in CO as a tracer of the magnetic field will introduce a systematic error unless the CP of CO lines are also measured.

The main goal of this paper is to find further evidence of CP in more objects and molecular lines through a search of archival data of the Submillimeter Array (SMA[1]). In Section 2 we discuss the issues that arise when doing polarimetry with radio interferometry, focusing specifically on circular polarization (CP). Section 4 presents archival observations of four objects made with the SMA on Mauna Kea and makes the case that these circular polarization detections are real and physical. Section 3 will give in detail our scheme for correcting a spurious source of CP that arises with the SMA. Finally in Section 5 we will highlight the significance of these CP detections and summarize relevant research.

2. MEASUREMENT OF CP WITH RADIO INTERFEROMETRY

The measurement of circular polarization is challenging to calibrate, especially when using radio interferometers like the SMA or ALMA. The SMA polarimeters use a quarter-waveplate (QWP) usually to convert incident LP light to CP light to measure LP signals. While not its most common use, at the SMA, the QWP can work the other way to measure CP: incident CP is converted to LP and then measured by the receivers. ALMA on the other hand uses linear feeds and measures the linearly polarized light directly. While both types of feeds can be used to measure CP, the calibration process is different Sault et al. (1996). While ALMA does not yet support measuring Stokes V reliably, the SMA has been used to take precise measurements of CP in Sgr A* (Muñoz et al. 2012). For a discussion on measuring CP with radio interferometry and on design choices at the SMA (such as the choice of converting from linear- to circular-polarization and vice-versa) see Hamaker et al. (1996); Marrone et al. (2008).

2.1. *Linear vs. Circular Feeds*

To illustrate briefly the differences between the two feed types consider the following: with an orthogonal circular polarization basis, the Stokes V parameter for a beam of light is defined by $V = \langle E_L^2 \rangle - \langle E_R^2 \rangle$, where E_L and E_R are the left-CP and right-CP electric fields, respectively. With an orthogonal linear basis Stokes V is defined by $V = -2\mathrm{Im}(E_x E_y^*)$ where E_x and E_y are the LP fields, and Im() denotes the imaginary part. In the CP case we take the difference of two measured intensities while the linear feed case requires us to measure the phase of the electromagnetic wave.

Now, when the measurement is made with interferometry it is the visibilities – the correlated waveforms between a pair of antennas – that are measured. In the CP case the Stokes V visibility scales as $\mathcal{V}_\mathrm{V} \propto \mathcal{V}_{RR} - \mathcal{V}_{LL}$ where $\mathcal{V}_{RR}$ and $\mathcal{V}_{LL}$ are the visibilities obtained from correlating two antenna measuring right-CP and left-CP, respectively (see eq. (3) below). In the linear feed case the Stokes V visibility is coupled with the Stokes Q and U visibilities (see Section 4.1 of Thompson et al. 2001). This means the Stokes Q and U of any calibration object must be measured as well. This is not possible with the SMA setup.

3. SQUINT CORRECTION

We now describe spurious Stokes V signals that can arise during observations such as those presented here and our scheme for correcting it. This instrumental Stokes V comes from a slight pointing offset between the left- and right-handed CP beams.

The archival data used was in all cases observed with the goal of measuring LP (i.e., the Stokes Q and Stokes U parameters). On the SMA this is done with a quarter-waveplate placed in front of the linear receivers to convert incident CP (LP) to LP (CP). While this method suffers from the errors that arise when subtracting two large measurements from each other, when performing CP measurements, it avoids having to solve for the LP terms of calibration objects (Marrone et al. 2008; Thompson et al. 2001).

The output of an interferometer are the visibilities. A visibility is the cross-correlation between the voltage signals from a pair of antennas and can be written as

$$\mathcal{V}(u,v) = \frac{r}{A_0 \Delta\nu} = \frac{\langle V_a(t) \star V_b(t) \rangle}{A_0 \Delta\nu} \qquad (1)$$

where A_0 is the collecting area of the antennas, $\Delta\nu$ is the bandwidth, and $r = \langle V_a(t) \star V_b(t) \rangle$ is the output of the correlator which is the time-averaged cross-correlation of voltage signals $V_a(t)$ and $V_b(t)$ from antenna a and b, respectively. The arguments u and v are determined by the baseline separation of the two antennas. Thus a pair of antennas samples a single point of the visibility function $\mathcal{V}(u,v)$ (Thompson et al. 2001).

Through the van Cittert-Zernike theorem it can be shown that the visibility function $\mathcal{V}(u,v)$ gives the Fourier transform of the source intensity $I(l,m)$ for angular position l and m (chap. 3 of Thompson et al.

[1] The Submillimeter Array is a joint project between the Smithsonian Astrophysical Observatory and the Academia Sinica Institute of Astronomy and Astrophysics and is funded by the Smithsonian Institution and the Academia Sinica.

2001). Thus we have

$$\mathcal{V}(u,v) = \int\int e^{-iul} e^{-ivm} I(l,m) dl dm. \quad (2)$$

Obtaining Stokes V from the visibilities measured with circular feeds is done as follows.

Given antennas a and b, the Stokes V visibility in the circular feed case is given by(Muñoz et al. 2012):

$$\mathcal{V}_V \simeq \frac{1}{2}\Big\{\mathcal{V}_{RR}/(g_{Ra}g^*_{Rb}) - \mathcal{V}_{LL}/(g_{La}g^*_{Lb})\Big\}, \quad (3)$$

where $\mathcal{V}_{RR}$ and $\mathcal{V}_{LL}$ are the right-handed CP and left-handed CP visibilities, respectively, and are measured by orienting the quarter-waveplate that is placed in the beam of the antennas and correlating the antenna responses (Marrone et al. 2008). The complex gain factors for each polarization for each antenna are g_{Ra}, g_{Rb}, g_{La} and g_{Lb} where R and L are for right- and left-CP, respectively. Because the Stokes V visibility is found by taking the difference of two beams a slight offset gives rise to pairs of positive and negative peaks of Stokes V, as can be seen in Figure 1 for example. This offset likely arises because of slight differences in the index of refraction of the quarter-waveplate when it is rotated.

To correct this offset we first note that since the visibilities are the Fourier transform of the intensity map, an offset in image space results in a complex factor in visibility space that can be absorbed into the gain coefficients.

To see this, consider a map $I(l,m)$ that represents the true intensity I at angular position l and m. If the instrument introduces an arbitrary offset to position (l_0, m_0), then the final image we calculate is shifted such that $I'(l,m) = I(l-l_0, m-m_0)$ and the measured visibility of the shifted map becomes

$$\begin{aligned}
\mathcal{V}'(u,v) &= \int\int e^{-iul} e^{-ivm} I(l-l_0, m-m_0) dl dm \\
&= \int\int e^{-iu(\alpha+l_0)} e^{-iv(\delta+m_0)} I(\alpha,\delta) d\alpha d\delta \\
&= e^{-iul_0} e^{-ivm_0} \int\int e^{-iu\alpha} e^{-iv\delta} I(\alpha,\delta) d\alpha d\delta \\
&= e^{-iul_0} e^{-ivm_0} V(u,v) \equiv g_{\rm offset} V(u,v) \quad (4)
\end{aligned}$$

where we used the change of variables $\alpha = l - l_0$ and $\delta = m - m_0$. We thus find the aforementioned complex factor that multiplies the true visibility $\mathcal{V}(u,v)$. It is therefore easiest to correct for the offset in visibility-space by using *Miriad* (Sault et al. 1995) to solve for the gain coefficients on each of the two polarized beams, independently of each other. Specifically the process is:

1. Observations are calibrated for gain and phase in the usual way using calibration observations of 'good' sources (usually quasars like 3C84, 3C454, etc.) (See Miriad User Guide Sault et al. (2008)).

2. Visibilities are split into line-free continuum data and line data. These are then mapped and used to obtain CLEAN models.

3. The separate continuum and line data are further split into LL and RR visibilities. *Miriad*'s `selfcal` is used on the continuum data to solve for the gain coefficients of each antenna and each polarization (L or R). This is done by minimizing the difference between measured visibilities $\mathcal{V}_{ij}$ of antennas i and j and model visibilities $\hat{\mathcal{V}}_{ij}$ according to $\epsilon^2 = \sum |\mathcal{V}_{ij} - g_i g_j^* \hat{\mathcal{V}}_{ij}|^2$ for each of the correlations LL and RR (Sault et al. 2008; Schwab 1980). The model visibilities used are those found earlier. Note the subscripts here denote a specific antenna and not the polarization as before.

4. The gains found from the continuum LL data is then applied to the line LL data, and similarly for the RR continuum and line data.

5. The different visibilities (LL, RR, RL, LR) are recombined and inverted to produce corrected maps. Spectra can be obtained either from the corrected visibilities or the maps.

Figure 1 shows maps before and after this correction is applied for the continuum in Orion KL around 345GHz. We see that before correction there are four large peaks of Stokes V, and that the two positive peaks have a negative peak close by. After the correction, though there are still noisy Stokes V signals throughout the image, the four peaks from before have completely disappeared.

4. OBSERVATIONS

We collected radio interferometric polarimetry observations from the Submillimeter Array (SMA) archive that had been measured using the circular feeds, a similar setup to that used by Muñoz et al. (2012) to measure circular polarization in Sgr A*. Because the archival observations were not taken with measurements of circular polarization in mind the SNR is often low, and we had to average velocity channels to increase it at the cost of spectral resolution. This generally increases the SNR from 3-4 to 6-10.

The four objects we present here are Orion KL, NGC7538, IRAS2A in NGC1333 and IRC+10216. The first three are well-known star-formation regions, while IRC+10216 is an evolved carbon star. We find significant Stokes V signals in all objects except for NGC1333. Table 1 shows a summary of the objects presented and related information.

The visibility data are corrected for beam squint, as explained in Section 3 in order to reduce spurious Stokes V signals. As previously mentioned squint typically

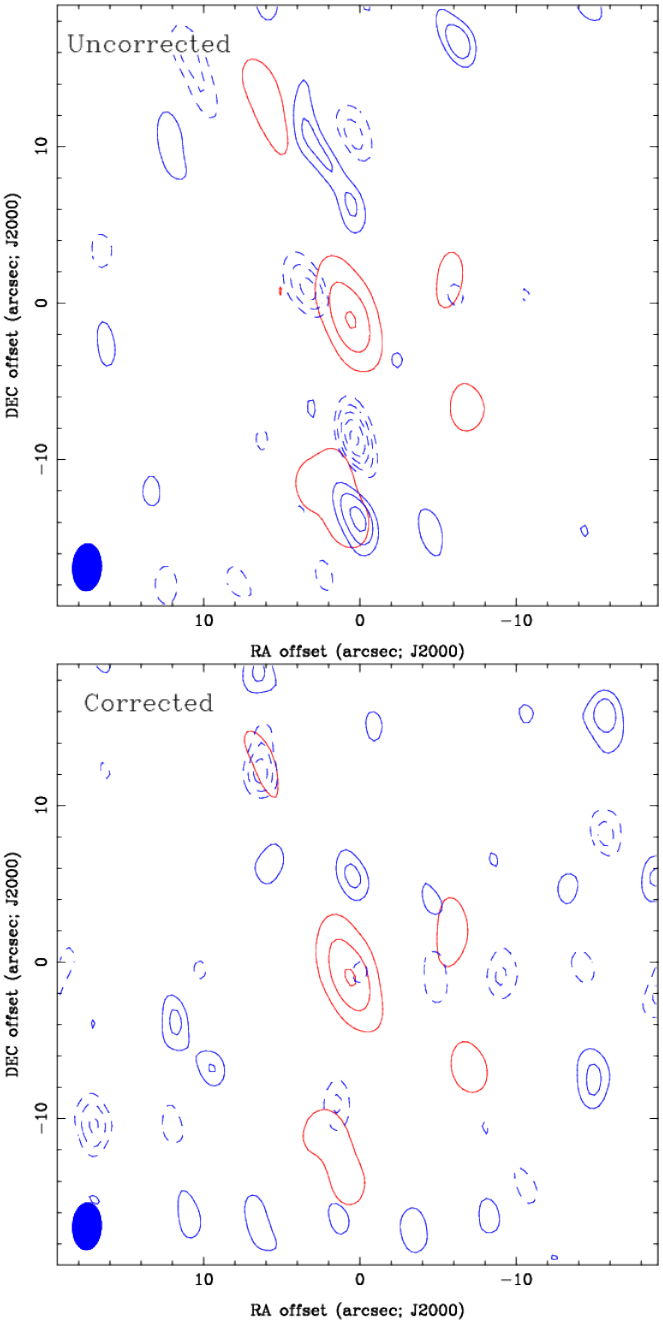

Figure 1. Map of the continuum around 345GHz in Orion KL before (top) and after (bottom) squint correction. Red contours are Stokes I, blue contours are Stokes V. Dashed lines denote negative values, solid lines denote positive values. Note the multiple pairs of positive and negative Stokes V peaks in the uncorrected map. These largely disappear after correction. The contour scales on both maps are identical. Red Stokes I contours are at 15%, 35%, 55%, 75% and 95% of the peak intensity. Blue Stokes V contours are at -8, -7, -6, -5, -4, -3, -2, 2, 3, 4, 5, 6, 7 and 8σ levels.

causes distinct pairs of positive and negative peaks of Stokes V throughout the inverted image. The squint correction is confirmed visually by inspecting the Stokes V maps, where we see the pairs of peaks largely disappear.

Object	Coordinates (J2000)	Array Configuration	Date Observed
Orion KL	RA $05^h35^m14.501^s$ Dec -05°22'30.40"	Compact	2008-01-06
NGC7538	RA $23^h13^m44.771^s$ Dec +61°26'48.85"	Compact	2014-10-28
IRC+10216	RA: $09^h47^m57.381^s$ Dec +13°16'43.70"	Compact	2009-11-24
NGC1333	RA $03^h28^m55.580^s$ Dec +31°14'37.10"	Compact	2010-10-14

Table 1. Summary of Archival Observations Used

Figures 2 and 3 show corrected Stokes I and Stokes V spectra (left) obtained at the peak of the CO ($J = 3 \rightarrow 2$) Stokes V signal on the corresponding maps (right). A comparison of Stokes V spectra before and after correction are shown in Figure 4. Notice in all cases the Stokes V signal decreases after squint correction. Stokes V can also be found in the average spectrum obtained from all the visibility data, though the significance is 3-5σ in that case compared to approximately 6-10σ when the spectra is taken from the inverted maps. The presence of a Stokes V signal in the visibilities indicates the detections are not simply the result of the inversion process that creates the maps. That is, the Stokes V signals are not due to sidelobes that appear when calculating the inverse Fourier transform of the visibilities. As can be seen in the maps, in general the peaks of Stokes I and Stokes V do not coincide.

In Orion KL the lines of CO ($J = 3 \rightarrow 2$ at 345.8GHz) and SiO ($J = 8 \rightarrow 7$ at 347.3GHz) are both bright (a peak Stokes I of around 20 Jy/beam and 55 Jy/beam respectively; not shown) and both show Stokes V signals. The CO Stokes V signal has an antisymmetric structure. On the other hand, Figure 5 shows the peak SiO Stokes V signal is purely negative.

In IRC+10216 we again see Stokes V in the CO ($J = 3 \rightarrow 2$) but also several signals in CS ($J = 7 \rightarrow 6$), SiS ($J = 19 \rightarrow 18$), and $H^{13}CN$ ($J = 4 \rightarrow 3$). These lines and their frequencies are listed in Table 2.

In NGC7538 the Stokes V signal in CO ($J = 3 \rightarrow 2$) at 345.8 GHz decreased in intensity after correction but is still extremely prominent. There was also a very strong Stokes V signal in CH_2CO at 346.6 GHz but it completely disappeared after correction.

Finally Figure 3 shows no detection in NGC1333, with only a weak detection of CO in Stokes I.

As mentioned previously, when assessing the Stokes V detections we consult the map for obvious pairs of positive/negative peaks that would indicate beam offset

Object	Line	(GHz)	Stokes V (Jy/beam)
Orion KL	CO ($J = 3 \rightarrow 2$)	345.8	0.65
	SiO ($J = 8 \rightarrow 7$)	347.3	-0.65
NGC7538	CO ($J = 3 \rightarrow 2$)	345.8	0.85
IRC+10216	CS ($J = 7 \rightarrow 6$)	342.88	0.6
	SiS (J =19→18)	344.78	0.2
	$H^{13}CN$ (J =4→3)	345.34	0.8
	CO ($J = 3 \rightarrow 2$)	345.8	0.4
NGC1333 (IRAS2a)	CO ($J = 3 \rightarrow 2$)	345.8	None

Table 2. Summary of corrected Stokes V signals found. The beam size is determined by the configuration of the antennas array. An intensity for the peak of the Stokes V signal is only given if the peak is noticeably higher than the noise level. The intensity quoted for CO in NGC7538 is before smoothing is applied.

and therefore a false Stokes V signal. The maps are integrated over a narrow frequency band of approximately 2 MHz so any peaks that exist are not washed out by noise in adjacent channels. In the maps for Orion KL and IRC+10216 shown in Figure 2 there are no negative peaks around the peak of Stokes V. However in NGC7538 there is quite a large negative Stokes V peak near our chosen peak that may indicate squint. The top panel of Figure 1 shows what 'squint peaks' look like (we know these peaks are from squint because they disappear after correction) and the pairs tend to resemble each other in shape. The pair of peaks around our chosen peak in NGC7538 however have distinct shapes. The worst case here is that the signal is entirely squint but on the other hand the signal may be a mixture of real and heavily affected by squint. The detections in Orion KL and IRC+10216 are more reliable.

5. DISCUSSION

The first question to address is whether our CP detections are real or result from instrumental artifacts. This is our chief concern because of the difficulty of calibrating CP measurements, especially since the observations presented here were not made with any special considerations for calibrating CP as in the observation of Sgr A* reported in Muñoz et al. (2012). We will repeat here the arguments made in Section 4 in support for the soundness of these detections. We then discuss earlier detections of CP and summarize how ARS can explain the detections presented in this work.

Firstly, we take the average of all the visibility data and note that the peak Stokes V is not proportional to the peak Stokes I at any particular frequency. For example, a large Stokes I at 347.25GHz does not indicate a corresponding peak in Stokes V. This property indicates that there is no significant leakage of Stokes I into Stokes V. This is true in Orion KL, where CO ($J = 3 \rightarrow 2$) and SiO ($J = 8 \rightarrow 7$) are the strongest lines, and the SiO ($J = 8 \rightarrow 7$) line is stronger. Therefore, if the Stokes V signal were purely leakage from Stokes I then we would expect to see an SiO Stokes V signal that is stronger than the CO Stokes V signal in the visibilities, but we do not; the Stokes V signal from CO ($J = 3 \rightarrow 2$) is stronger. This is also true in the visibilities of IRC+10216, where the CS ($J = 7 \rightarrow 6$) and SiS ($J = 19 \rightarrow 18$) lines have similar strengths but the Stokes V at SiS ($J = 19 \rightarrow 18$) is twice as intense. However, in the same object $H^{13}CN$ ($J = 4 \rightarrow 3$) and CO ($J = 3 \rightarrow 2$) have Stokes V intensities that appear proportional to their Stokes I intensity (stronger I means stronger V).

We also note that for Orion KL the shapes of the Stokes V signals vary across the frequency band and interpret this to mean that the signals are not instrumental in nature, assuming that any instrumental mechanism for producing spurious Stokes V produces a single type of CP (left or right). For example Figure 5 shows a spectrum for that source with Stokes V in CO and SiO. The SiO signal is purely negative (indicating only left-circular polarization) but the CO signal is antisymmetric, indicating the presence of both LCP and RCP. This has a physical explanation using the ARS model in terms of blue-shifted and red-shifted scattering populations that will be considered in Section 5.2. We know of no instrumental mechanism for producing such a signature. For the other objects the Stokes V signal is always positive.

In the case of IRC+10216, an evolved carbon star with an extended envelope, we note that the peak of Stokes V in the CO ($J = 3 \rightarrow 2$) map (bottom-right panel of Figure 2) is roughly 6" away from the Stokes I emission, and were concerned that the Stokes V peak was not even on the object. From single-dish CO ($J = 2 \rightarrow 1$) observations of the shell around IRC+10216 we find the radius of the CO shell to be 50" (Fig. 1 of Cernicharo et al. 2015), indicating that the Stokes V signal is indeed on the object.

Spatial filtering due to the resolution of the interferometer explains the much smaller radius of IRC+10216 in the observations presented here and also explains the frequent occurences of negative Stokes I in almost all the spectra shown in Figures 2, 3, and 5, as well as the extremely high levels of CP that range from 6% to 30%. The largest resolvable object by an interferomter is determined by the length of the shortest baseline, meaning that large scale emission can be invisible to the interfer-

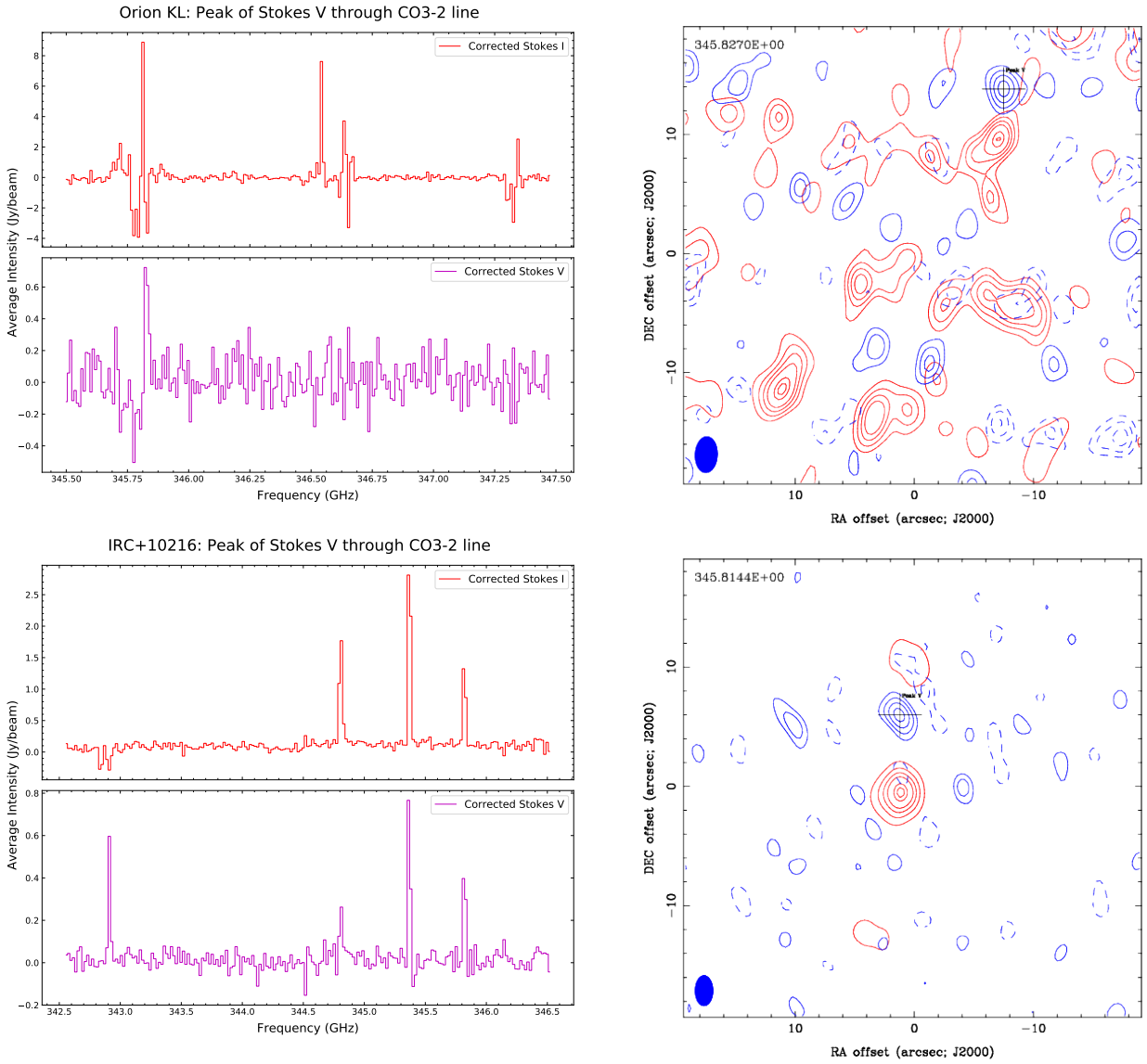

Figure 2. Corrected spectra and maps of the CO ($J = 3 \rightarrow 2$) line (345.8GHz) for Orion KL and IRC+10216. ***Spectra*:** *Miriad*'s `maxfit` is used on the CO map to obtain the location on the image where the Stokes V signal at 345.8GHz is maximum, and a spectrum is obtained through that point. The cross on the map denotes the location of that peak. The red line is Stokes I and the blue is Stokes V. ***Maps*:** Blue contours are Stokes V and are shown at the -4, -3, -2, 2, 3, 4σ levels. The RMS error for each Stokes V map is found using *Miriad*'s `imstat` command: $\sigma = 0.30$ and 0.17 Jy/beam, for Orion KL and IRC+10216, respectively. Dark red contours are Stokes I and the levels are 15%, 30%, 45%, 60%, 85% and 95% of the maximum. The value in the top left is the central frequency of the mapped signal and the map is integrated over a narrow bandwidth of $\sim$2 MHz.

ometer. For example in Orion KL the CO ($J = 3 \rightarrow 2$) Stokes I emission is large and extended. If then the Stokes V signal comes from smaller more localized areas, we would observe peaks of Stokes V as shown and only a portion of the Stokes I that is present. The rest of the Stokes I signal would be filtered away which could shift the zero-level to smaller values. Fluctuations in Stokes I would then appear to have negative values. The smaller Stokes I would also explains the high levels of V/I observed.

Finally we checked and confirmed that there were no Stokes V signals in the continuum larger than those found at molecular lines like CO and SiO. If the detected CP originates from instrumental artifacts then we would detect CP at similar levels in the continuum, but this is not seen. The level of CP found at molecular transitions is always higher than the level of CP in the continuum for the observations presented here.

We therefore feel confident that the CP reported here, although perhaps suffering from some level of instrumental contamination, is real and originate from each of these objects. It is thus important to improve the measurement and calibration of CP for future studies of magnetic fields using polarimetry.

5.1. *Earlier Detections*

Circular polarization in a molecular spectral line weakly sensitive to the Zeeman effect was first reported in Houde et al. (2013), where roughly 2% CP was de-

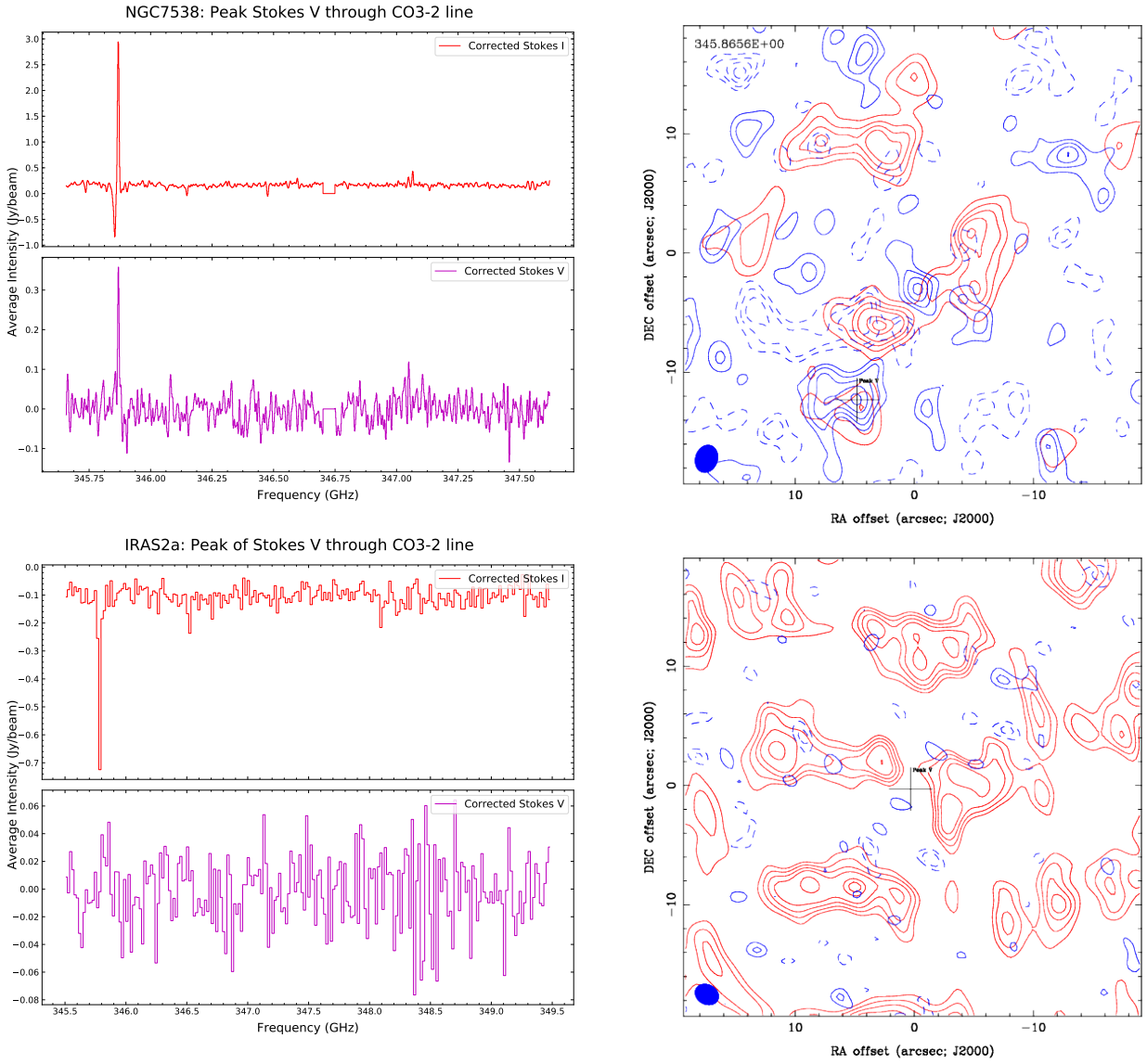

Figure 3. Same as Figure 2 but for NGC7538 and NGC1333 (IRAS2A). The spectrum for NGC7538 is Hanning smoothed. No significant Stokes V signal is detected in NGC7538, probably because the object is too dim. Contours are the same levels as in Figure 2 and the spectrum is obtained the same way. The RMS for the NGC7538 map is $\sigma = 0.15$ Jy/beam.

tected in the ^{12}CO ($J = 2 \rightarrow 1$) transition at 230.5 GHz in Orion KL using the FSPPol at the CSO. The CP signal was approximately symmetric (i.e. "∩"-shaped). The observation was repeated three months after the first measurement to confirm the result was not spurious, with similar results. Additionally the strong line of HCN ($J = 3 \rightarrow 2$) at 265.9 GHz in Orion KL was measured and no CP higher than the 0.1% level was detected. The detection in CO and the absence of a detection in HCN indicates that the FSPPol/CSO observations were not suffering from leakage into Stokes V and highlights the CO molecule as a source of non-Zeeman CP. In all the objects presented here we find CP in ^{12}CO ($J = 3 \rightarrow 2$) at 345.8 GHz (except for in NGC1333 where the CO line is weak). This is consistent with the original 2013 detection.

In follow up work Hezareh et al. (2013) examined the supernova remnant IC 443 using dust polarimetry with PolKa at APEX and polarization maps of ^{12}CO ($J = 2 \rightarrow 1$) and ($J = 1 \rightarrow 0$) taken with the IRAM 30m telescope. They found that initially the linear polarization maps of dust and CO differed greatly in their polarization angles. Expecting that there was conversion of linear to circular polarization due to ARS, the CO Stokes V fluxes were then reinserted into the CO LP signals. The resulting CO polarization angle maps then agreed very well with each other as well as with the dust map (Fig. 9 of Hezareh et al. 2013). This result clearly establishes a conversion from linear to circular polarization.

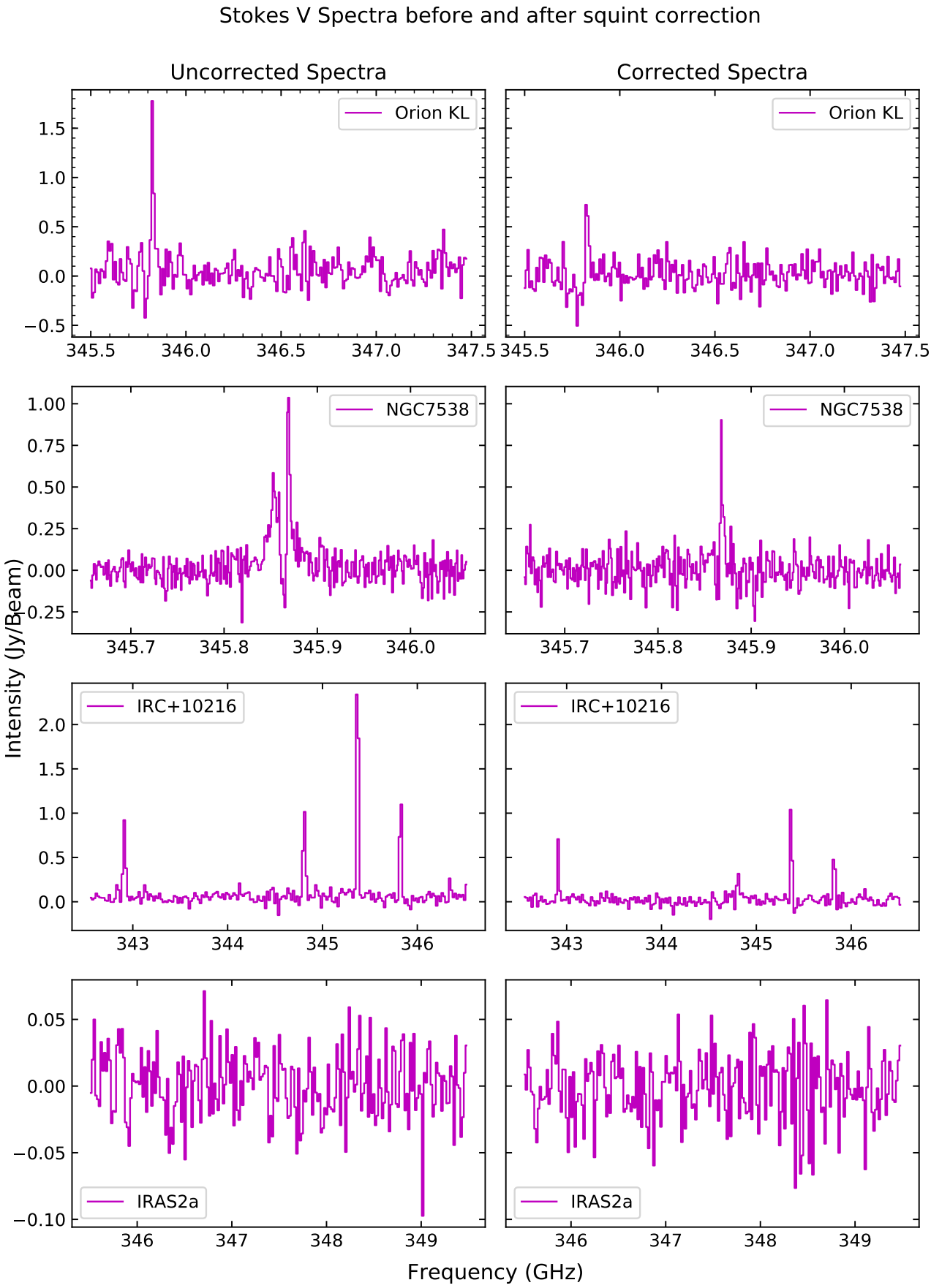

Figure 4. Stokes V spectra of all objects before and after squint correction. *Miriad*'s `maxfit` is used on the CO map for each respective object to obtain the location in the image where the Stokes V signal at 345.8GHz is maximum, and a spectrum is obtained through that point. Note that the Stokes V signal decreases in all cases after squint correction.

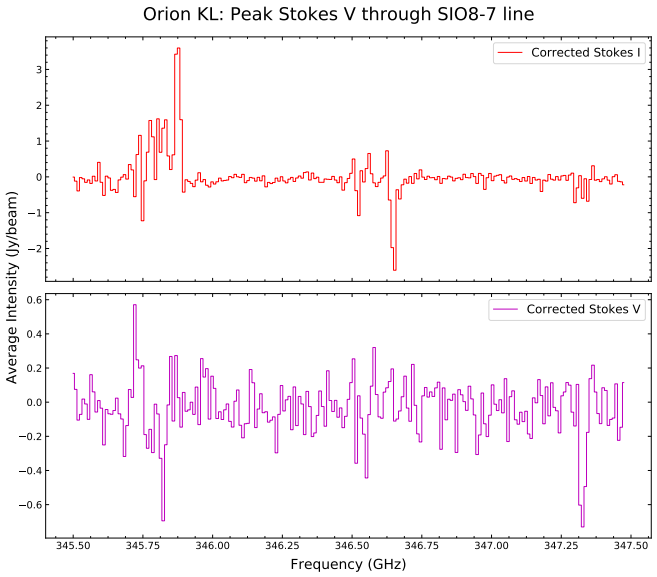

Figure 5. Peak Stokes V signal for the SiO ($J = 7 \rightarrow 8$ at 347.3 GHz) transition in Orion KL. Note there is also a strong Stokes V signal in the CO ($J = 3 \rightarrow 2$ at 345.8 GHz) transition here. The SiO signal is purely negative but the CO signal is antisymmetric.

5.2. *Anisotropic Resonant Scattering*

ARS was the mechanism first proposed by Houde et al. (2013) to explain the presence of CP in the transitions of CO, but failed to explain the observed positive and symmetric "∩"-shaped Stokes V profile. In a follow up paper Houde (2014) considered observations of Stokes V in SiO masers and showed that different profile shapes easily arose if there were populations of scattering foreground molecules slightly outside of the velocity range of the line. For example in that case a blue-shifted scattering population of molecules results in a negative "∪"-shaped profile and a red-shifted population results in a positive "∩"-shaped profile. The presence of both a blue- and red-shifted population results in an antisymmetric "S"-shaped profile like the one seen in the top left panel of Figure 2.

The basic principle of ARS can be illustrated by considering linearly polarized radiation oriented at some angle θ to the foreground magnetic field. The incident and scattered radiation can be written in terms of the n-photon states as (Houde et al. 2013)

$$|\psi\rangle = \alpha|n_{||}\rangle + \beta|n_{\perp}\rangle \quad (5)$$

$$|\psi'\rangle \simeq \alpha e^{i\phi}|n_{||}\rangle + \beta|n_{\perp}\rangle, \quad (6)$$

where $\alpha = \cos(\theta)$, $\beta = \sin(\theta)$ and ϕ is a phase shift incurred after multiple scattering events. Following the definitions of the Stokes parameters and using an appropriate basis the Stokes parameters for the scattered radiation can be found to be

$$I = \alpha^2 + \beta^2 \quad (7)$$

$$Q = \alpha^2 - \beta^2 \quad (8)$$

$$U = 2\alpha\beta\cos(\phi) \quad (9)$$

$$V = 2\alpha\beta\sin(\phi). \quad (10)$$

This implies that in the chosen basis Stokes U is lost to Stokes V. A calculation of the phase shift ϕ incurred due to ARS can be found in Houde et al. (2013).

Now, given a conversion from U to V it is clear that measuring V is necessary for techniques like the DCF method that rely on the dispersion of the PAs of LP to calculate the strength of the magnetic field. This is because without corresponding V measurements, the PAs obtained from a molecular spectral line subject to ARS (like CO ($J = 3 \rightarrow 2$)) will be rotated in a complicated way that changes the dispersion of the PAs, as seen in Hezareh et al. (2013). In that study the measured V was re-inserted into U according to

$$U' = U\cos\phi + V\sin\phi, \quad (11)$$

where $\phi = \tan^{-1}(V/U)$, to obtain corrected polarization angles. This was shown to work by comparing CO ($J = 2 \rightarrow 1$) polarization maps to dust continuum maps (which is not subject to ARS) and seeing that the two maps only agreed after correction.

Because the DCF method relies on the observed dispersion of PAs using LP from CO maps therefore yields the incorrect value for the magnetic field unless the PAs are corrected (Hezareh et al. 2013; Chandrasekhar & Fermi 1953; Hildebrand et al. 2009).

6. CONCLUSION

We analyzed polarimetric observations from the SMA archive of Orion KL, IRC+10216, NGC7538 and NGC1333 and examined them for CP signals. The data were corrected for squint, a source of false Stokes V signals that arises due to a slight misalignment in the beams used to obtain Stokes V when performing observations. We found evidence of significant Stokes V in Orion KL, IRC+10216 and NGC7538 in the transitions of CO ($J = 3 \rightarrow 2$), SiO ($J = 8 \rightarrow 7$), CS ($J = 7 \rightarrow 6$), SiS ($J = 19 \rightarrow 18$) and $H^{13}CN$ ($J = 4 \rightarrow 3$). We also obtained much higher percentages of polarization than expected (ranging from 6-30% for V/I) due to the spatial filtering of large scale emission.

Theories that explain the presence of non-Zeeman CP in molecular spectral lines rely on the conversion of background LP. The detections in multiple lines and objects presented here indicate that such an effect is likely widespread and common. The conversion of CP-to-LP modified the observed dispersion of PAs which alters the calculated magnetic field obtained from analyses like the

DCF method.

Taking precise observations of CP along with LP and correcting for this conversion effect is therefore a critical step in polarization studies of the magnetic field in the interstellar medium.

REFERENCES

Cernicharo, J., Marcelino, N., Agúndez M., & Guéllin, M. 2015 A&A, 575, A91

Chandrasekhar, S., & Fermi, E. 1953 ApJ, 118, 113

Crutcher, R. M. 2012 Annu. Rev. Astron. Astrophys, 50, 29-63

Goldreich, P., Kylafis, N. D. 1981 ApJ, 243, L75-L78

Hamaker, J. P., Bregman, J. D., & Sault, R. J. 1996 A&A Suppl. Ser., 117, 137-147

Hezareh, T. J., Wiesemeyer, H., Houde, M., Gusdorf, A., Siringo, G. 2013 A&A, 558, A45

Hildebrand, R. G., Kirby, L., Dotson. J. L., Houde, M., Vaillancourt, J. E. 2009 ApJ, 696, 567-573

Houde, M., Hezareh, T., Jones, S., & Rajabi, F. 2013 ApJ, 764, 24

Houde, M. 2014 ApJ, 795, 27

Muñoz, D. J., Marrone, D. P., Moran, J. M., & Rao, R. 2012 ApJ, 745, 115

Marrone D. P. & Rao R. 2008, Proc. SPIE 7020, 70202B

Sault, R. J., Teuben, P. J. & Wright M. C. H. 1995 ADASS IV, ASP Conference Series, 77, 433-436

Sault, R. J., Hamaker, J. P., & Bregman, J., D. 1996 A&A Suppl. Ser., 117, 149-159

Sault, R. J., Killeen, N. 2008, Miriad Users Guide, Australia Telescope National Facility

Schwab, F. R. 1980, Proc. SPIE 0231, Intl Optical Computing Conf I

Thompson, A. R., Moran, J. M., & Swenson Jr, G. W. 2001, Interferometry and synthesis in radio astronomy (John Wiley & Sons)

Vallée, J. P. 2011, New Astronomy Reviews 55, 23–90